Exclusive production of a large mass photon pair

Jakub Wagner

National Centre for Nuclear Research, Warsaw

based on:
A. Pedrak, B. Pire, L. Szymanowski and JW [PRD96 (2017)]
A. Pedrak, B. Pire, L. Szymanowski and JW [PRD101 (2020)]
O. Grocholski, B. Pire, P. Sznajder, L. Szymanowski and JW [PRD104 (2021)]
O. Grocholski, B. Pire, P. Sznajder, L. Szymanowski and JW [PRD105 (2022)]

REVESTRUCTURE workshop

Zagreb, Jul 10 - 12, 2023

NATIONAL CENTRE FOR NUCLEAR RESEARCH ŚWIERK

GPD extraction from exclusive experiments

- Deeply Virtual Compton Scattering: $e^- N \to e^- N\gamma$.
  The relevant hard sub-process: $\gamma^* N \to \gamma N$,

  $\to$ Many talks at this workshop :)

- Timelike Compton Scattering: $\gamma N \to \gamma^* N$,

  $\to$ See Marie Boër talk on Wednesday

- Double Deeply Virtual Compton Scattering: $\gamma^* N \to \gamma^* N$,

  $\to$ See Victor Martinez-Fernandez talk today

- Deeply Virtual Meson Production: $\gamma^* N \to M + N$,

  $\to$ See Goritschnig, Kishore, Čuić talks Tuesday and Wednesday

- Recently, processes with $2 \to 3$ hard sub-processes proposed:
  $\gamma^* N \to \gamma + M + N$

  $\to$ See Saad Nabeebaccus talk today

Why study this process?

The considered process:

- Photoproduction of photon pairs with large invariant mass:

$$\gamma\ N \to \gamma\ \gamma\ N$$

- The hard part is a $2 \to 3$ reaction, a new type of processes studied within the framework of QCD collinear factorization.
- The amplitude depends only on charge-odd combinations of GPDs (only valence quarks contribute):
  - **DVCS:** $\sum_q e_q^2 \left(H^q(x,\xi) - H^q(-x,\xi)\right)$ and $H^g(x)$
  - **Diphoton:** $\sum_q e_q^3 \left(H^q(x,\xi) + H^q(-x,\xi)\right)$ and no gluons
- No contribution from the badly known chiral-odd quark GPDs at the leading twist.

Factorisation proven - Zhite Yu's talk at DIS23

Classification of GPD processes

- Electro-production (JLab, EIC, ...)

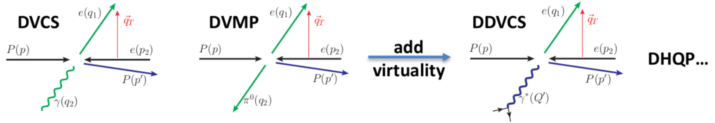

- Photo-production (JLab Hall-D, ...)

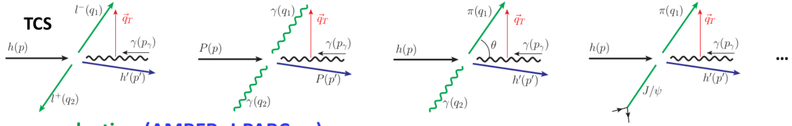

- Meso-production (AMBER, J-PARC, ...)

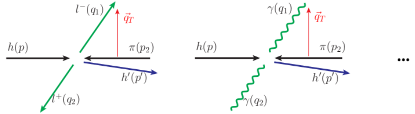

Proved factorization generally
[Qiu, Yu, PRD 107 (2023), 014007]

Kinematics

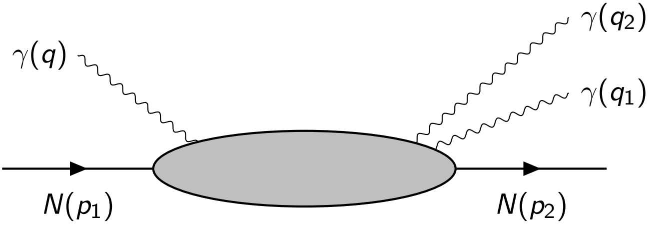

$$S_{\gamma N} = (p_1 + q)^2, \qquad u' = (q_2 - q)^2,$$

$$M^2_{\gamma\gamma} = (q_1 + q2)^2, \qquad t = (p_1 - p_2)^2.$$

$$\xi \approx \frac{M^2_{\gamma\gamma}}{2S_{\gamma N}}.$$

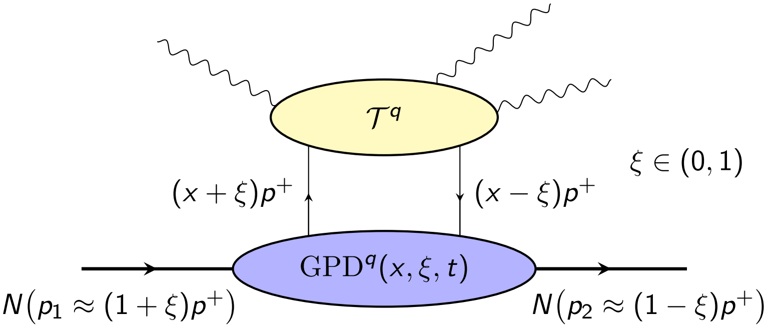

The full amplitude:

$$\mathcal{T} = \sum_q \int_{-1}^{1} dx\, \mathcal{T}^q\big(x,\xi,\ldots\big)\mathrm{GPD}^q(x,\xi,t).$$

The leading order analysis

Pedrak et al. Phys. Rev. D 96 (2017) [arXiv:1708.01043]

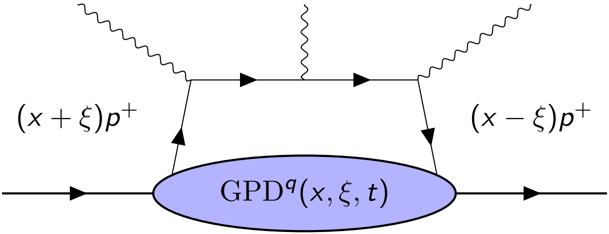

LO results

The process can be studied at intense quasi-real photon beam facilities in JLab or EIC.

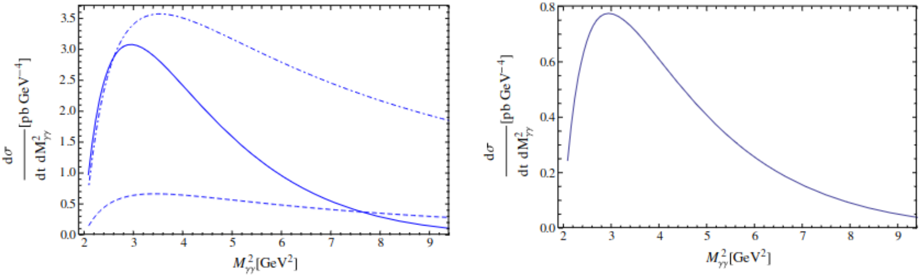

FIG. 5. The $M^2_{\gamma\gamma}$ dependence of the unpolarized differential cross section $\frac{d\sigma}{dM^2_{\gamma\gamma}dt}$ on a proton (left panel) and on a neutron (right panel) at $t = t_{\min}$ and $S_{\gamma N} = 20$ GeV^2 (full curves), $S_{\gamma N} = 100$ GeV^2 (dashed curve) and $S_{\gamma N} = 10^6$ GeV^2 (dash-dotted curve, multiplied by 10^5).

Next-to-leading order results

NLO factorization and the amplitude

Phys. Rev. D 104 (2021) [2110.00048]

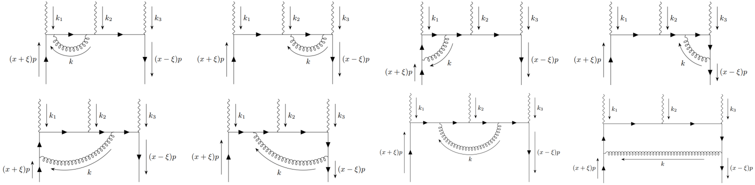

Figure: Considered 1-loop diagrams

Next-to-leading order results

- 2- and 3-point loops → relatively simple results.
- 5-point loop integral can be reduced to a sum 4-point ones.
- Finite part of a 4-point diagrams: expressible in terms of

$$\mathcal{F}_{nab} := \int_0^1 dy \int_0^1 dz\, y^a z^b \Big(\alpha_1 y + \alpha_2 z + \alpha_3 yz + i\epsilon\Big)^{-n},$$

$$\mathcal{G} := \int_0^1 dy \int_0^1 dz\, z^2 \Big(\alpha_1 y + \alpha_2 z + \alpha_3 yz + i\epsilon\Big)^{-2} \times \log\Big(\alpha_1 y + \alpha_2 z + \alpha_3 yz + i\epsilon\Big).$$

Large computational power is needed to get stable results.

PARTONS

PARtonic Tomography Of Nucleon Software
B. Berthou et al., Eur. Phys. J. C 78, 478 (2018),
hep-ph/1512.06174

http://partons.cea.fr

Considered GPD models

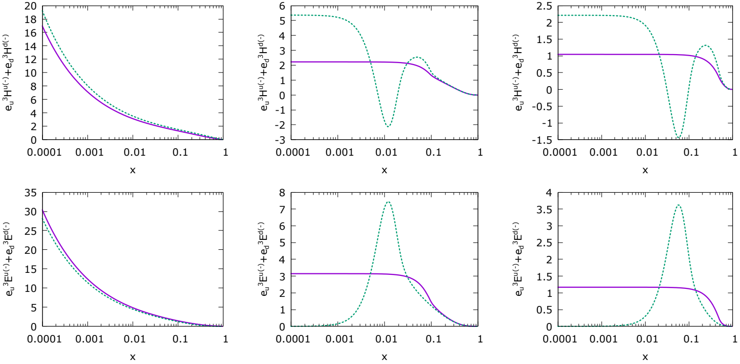

Figure: Comparison between GK [hep-ph/0708.3569] (solid magenta) and MMS [hep-ph/1304.7645] (dotted green) GPD models for $t = -0.1\ \mathrm{GeV}^2$ and the scale $\mu_F^2 = 4\ \mathrm{GeV}^2$ for
$\xi = x$ $\quad$ $\xi = 0.1$ $\quad$ $\xi = 0.5$.

H^q, E^q - vector GPDs, $\tilde{H}^q, \tilde{E}^q$ - axial GPDs.

$$\mathcal{H} = \sum_q \int_{-1}^{1} dx\, \mathcal{T}^q(x, \xi, ...) H^q(x, \xi, t),$$

$\mathcal{E}, \tilde{\mathcal{H}}, \tilde{\mathcal{E}}$ defined in the analogous way.

Contribution from axial GPDs is small at LO, we neglect it in the NLO analysis.

Stability of results

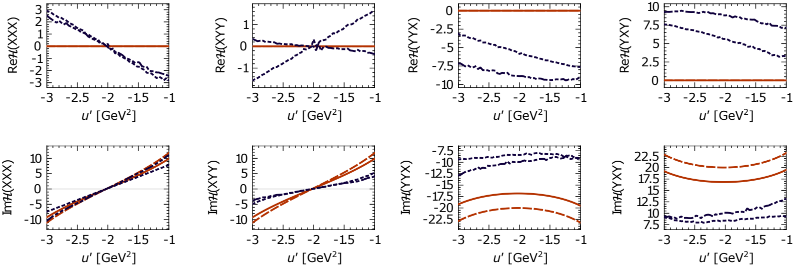

Figure: $\mathcal{H}$ as a function of u' for $S_{\gamma N} = 20\ \mathrm{GeV}^2$, $M^2_{\gamma\gamma} = 4\ \mathrm{GeV}^2$ (which corresponds to $\xi \approx 0.12$) and $t = t_0 \approx -0.05\ \mathrm{GeV}^2$.

LO: solid (dashed) red line,
NLO: dotted (dash-dotted) blue line
for GK (MMS) GPD model

Stability of results

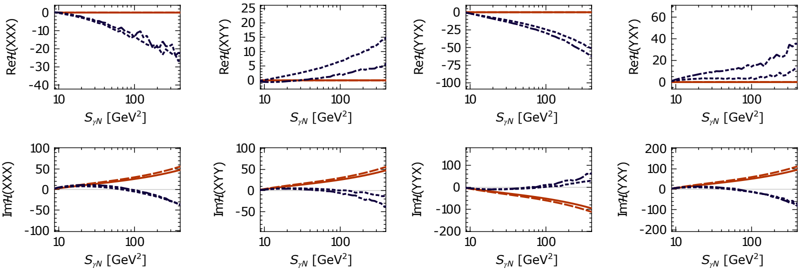

Figure: $\mathcal{H}$ as a function of $S_{\gamma N}$ for $M^2_{\gamma\gamma} = 4\ \mathrm{GeV}^2$, $t = t_0$ and $u' = -1\ \mathrm{GeV}^2$.

LO: solid (dashed) red line,
NLO: dotted (dash-dotted) blue line
for GK (MMS) GPD model

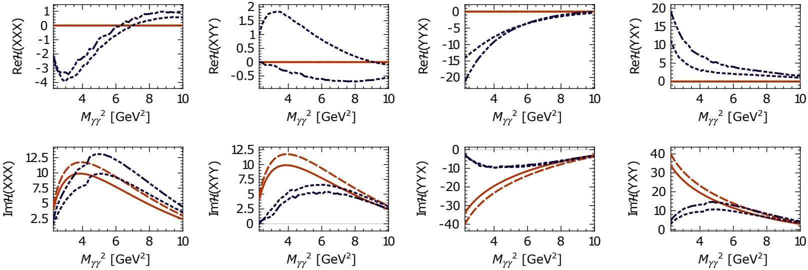

Figure: $\mathcal{H}$ as a function of $M_{\gamma\gamma}$ for $S_{\gamma N} = 20\ \mathrm{GeV}^2$, $t = t_0$ and $u' = -1\ \mathrm{GeV}^2$.

LO: solid (dashed) red line,
NLO: dotted (dash-dotted) blue line
for GK (MMS) GPD model

$$\frac{d\sigma}{dt\,du'\,dM^2_{\gamma\gamma}}$$

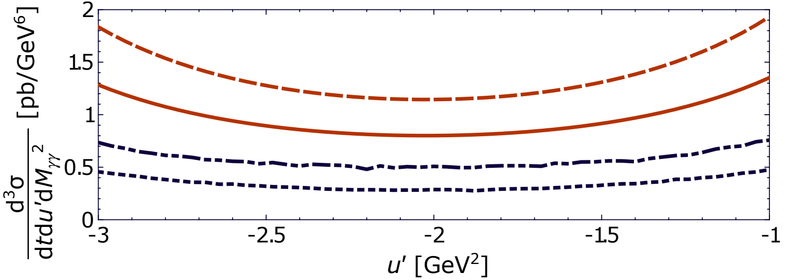

Figure: Differential cross-section as a function of u' for $S_{\gamma N} = 20\ \mathrm{GeV}^2$, $M^2_{\gamma\gamma} = 4\ \mathrm{GeV}^2$ ($\xi \approx 0.12$) and $t = t_0 \approx -0.05\ \mathrm{GeV}^2$ for proton target.

LO: solid (dashed) red line,
NLO: dotted (dash-dotted) blue line
for GK (MMS) GPD model.

Differential cross section: $S_{\gamma N}$-dependence

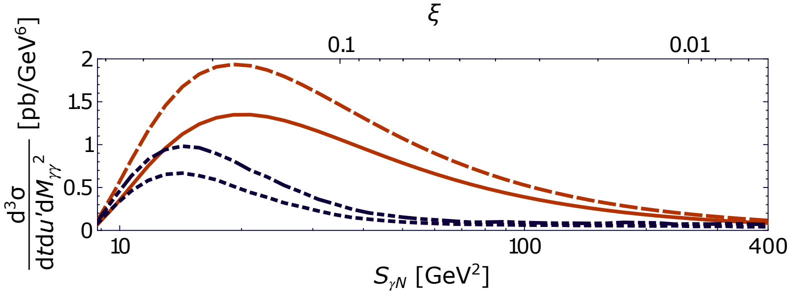

Figure: Differential cross-section as a function of $S_{\gamma N}$ (bottom axis) and the corresponding ξ (top axis) for $M^2_{\gamma\gamma} = 4~\mathrm{GeV}^2$, $t = t_0$ and $u' = -1~\mathrm{GeV}^2$.

LO: solid (dashed) red line,
NLO: dotted (dash-dotted) blue line
for GK (MMS) GPD model.

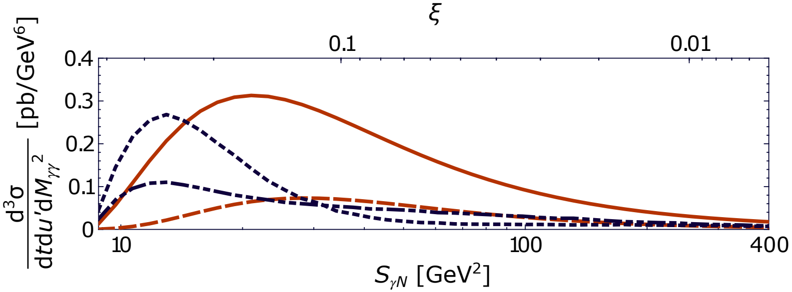

Figure: The same, but for neutron target.

LO: solid (dashed) red line,
NLO: dotted (dash-dotted) blue line
for GK (MMS) GPD model.

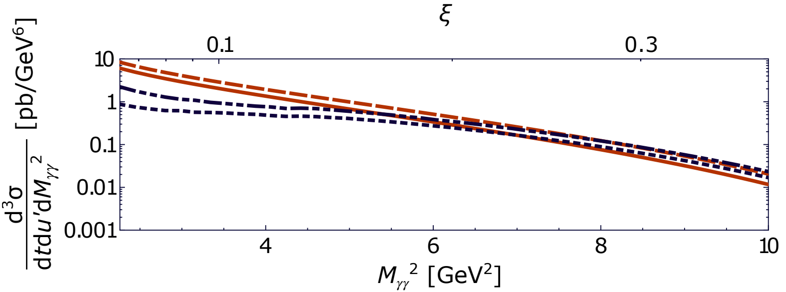

Figure: Differential cross-section as a function of $M^2_{\gamma\gamma}$ (bottom axis) and the corresponding ξ (top axis) for $S_{\gamma N} = 20\ \mathrm{GeV}^2$, $t = t_0$ and $u' = -1\ \mathrm{GeV}^2$.

LO: solid (dashed) red line,
NLO: dotted (dash-dotted) blue line
for GK (MMS) GPD model

Differential cross section: ϕ-dependence

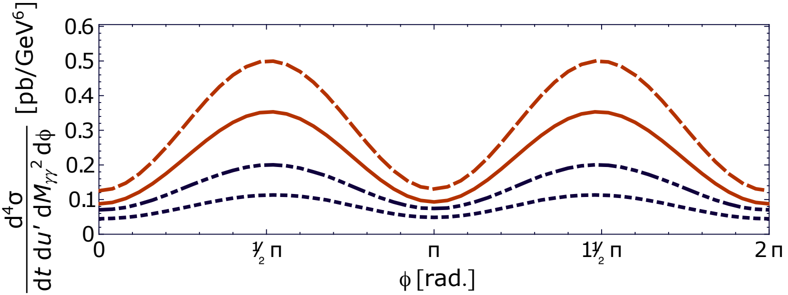

Figure: Differential cross-section as a function of ϕ – the angle between the initial photon polarization and one of the final photon momentum in the transverse plane for $S_{\gamma N} = 20\ \mathrm{GeV}^2$, $M^2_{\gamma\gamma} = 4\ \mathrm{GeV}^2$ (which corresponds to $\xi \approx 0.12$), $u' = -1\ \mathrm{GeV}^2$ and $t = t_0 \approx -0.05\ \mathrm{GeV}^2$.

LO: solid (dashed) red line,
NLO: dotted (dash-dotted) blue line
for GK (MMS) GPD model

MC simulations

Exclusive diphoton photoproduction

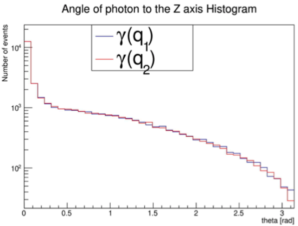

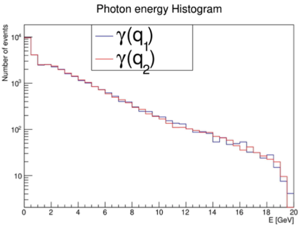

B. Skura (Warsaw U. of Technology), PS
preliminary results

- The process implemented in EpIC MC generator with equivalent-photon approximation

$$\frac{\mathrm{d}^6\sigma}{\mathrm{d}Q^2\,\mathrm{d}y\,\mathrm{d}t\,\mathrm{d}u'\,\mathrm{d}M^2_{\gamma\gamma}\mathrm{d}\phi} = \Gamma(y, Q^2)\times\frac{\mathrm{d}^4\sigma_{2\gamma}}{\mathrm{d}t\,\mathrm{d}u'\,\mathrm{d}M^2_{\gamma\gamma}\mathrm{d}\phi}$$

- Condition used in generation of events

E = 20 GeV	$0 < -t < 1$ GeV^2	$0 < y < 1$
	$0 < -u < 6$ GeV^2	$0 < Q^2 < 0.01$ GeV^2
	1 GeV^2 $< M_{\gamma\gamma}^2 <$ 5 GeV^2	
	$0 < \phi < 2\pi$	

- Event counts are scaled to 10 fb^{-1}

Electroproduction and Bethe-Heitler contributions

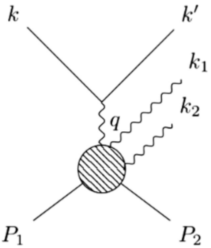

FIG. 1. The QCD process contributing to $eN \to e'\gamma\gamma N'$.

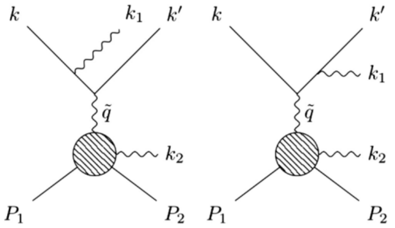

FIG. 2. The single Bethe-Heitler process contributing to $eN \to e'\gamma\gamma N'$. Two other graphs with $k_1 \leftrightarrow k_2$ interchange are not shown.

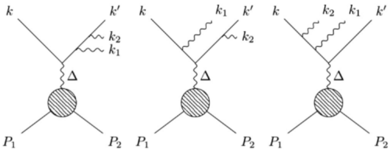

FIG. 3. The double Bethe-Heitler process contributing to $eN \to e'\gamma\gamma N'$. Three other graphs with $k_1 \leftrightarrow k_2$ interchange are not shown.

Bethe-Heitler contributions

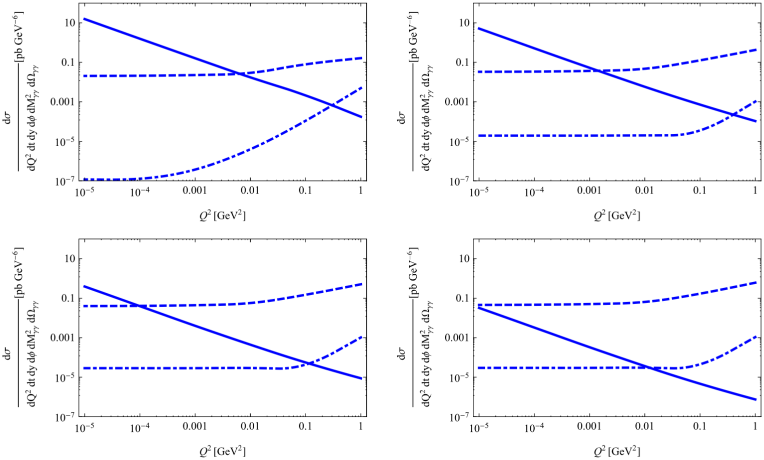

FIG. 10. The relative importance of the different processes contributing to $eN \to e'\gamma\gamma N'$—shown here (from left to right and from top to bottom) for $s = 20$ GeV^2, $s = 100$ GeV^2, $s = 1000$ GeV^2 and $s = 10000$ GeV^2 at the kinematical point $M^2_{\gamma\gamma} = 3$ GeV^2, $\theta_{\gamma\gamma} = 3\pi/8$, $\phi_{\gamma\gamma} = 0$, $y = 0.6$—depends much on the value of Q^2. The QCD process (solid curve) dominates at very low Q^2, the single Bethe-Heitler process (dashed curve) dominates at higher Q^2, while the double Bethe-Heitler process (dotted curve) is always subdominant.

Summary

- $\gamma N \to \gamma\gamma N$ can provide valuable information about charge-odd combinations of GPDs,
- We performed a next-to-leading order analysis of the diphoton photoproduction process,
- NLO corrections result in smaller cross sections,
- Due to complicated form of the NLO amplitude, a large computational power is needed to reduce the numerical noise.